IEEE Access
Multidisciplinary | Rapid Review | Open Access Journal

Received July 7, 2019, accepted August 7, 2019, date of publication August 22, 2019, date of current version September 11, 2019.

Digital Object Identifier 10.1109/ACCESS.2019.2936920

Influence of Various Magnetic Pole on Electromagnetic Performance of Consequent-Pole Permanent Magnet Machine

FENG LI, KAI WANG, (Senior Member, IEEE), HAIYANG SUN, AND JINWANG KONG
College of Automation, Nanjing University of Aeronautics and Astronautics, Nanjing 211106, China

Corresponding author: Kai Wang (k_wang@ieee.org)

This work was supported in part by the National Natural Science Foundation of China under Project 51607089, in part by the Natural Science Foundation of Jiangsu Province under Project BK20180016, in part by the Power Electronics Science and Education Development Program of the Delta Environmental and Educational Foundation under Grant DREK2019002, and in part by the Research Innovation of Graduate Student in Jiangsu Province under Grant KYCX17_0264.

ABSTRACT Permanent magnet (PM) machine with consequent pole (CP) rotor can improve the PM utilization ratio. However, one group PMs with the same polarity is replaced by iron core which deteriorating the electromagnetic performance of the machine, including even-order back-EMF harmonics, torque ripple, as well as unipolar leakage flux. Therefore, CP PM machine with various magnetic pole, i.e., equal pole-arc magnetic pole (EMP) and asymmetric magnetic pole (AMP) structure is proposed, with smaller torque ripple can be achieved, without deteriorating the torque ability compared with the conventional CP PM machine. Further, the influence of various CP PM magnetic pole on the end leakage flux is analyzed by three-dimensional (3-D) finite element (FE), which includes leakage flux distributions as well as magnetization of shaft. The electromagnetic characteristics of the machine with EMP and AMP rotor are compared with traditional surface-mounted and CP PM machines by FE analysis. It is demonstrated that EMP and AMP rotor structure can reduce even-order harmonics, torque ripple and end leakage flux for the machines. Finally, one prototype with CP AMP rotor is tested to confirm the theoretical and FE analysis, which includes suppression effect of even back-EMF harmonics, torque characteristics as well as leakage flux at the end shaft.

INDEX TERMS AMP, CP rotor, EMP, even-order back-EMF harmonic, PM machine, torque ripple, unipolar leakage flux.

I. INTRODUCTION

The PM machines can exhibit high torque density, high power density, high power factor and high efficiency owing to the employ of high magnetic energy product material (such as NdFeB), and are widely exploited in more-electric aircrafts, electric vehicles, and high-power wind generation systems [1], [2]. However, more and more researchers devote to the PM-less machines with the increasing concerns on energy crisis and rising prices of rare earth materials [3].

In order to improve the utilization of PM material and maintain excellent electromagnetic performance, the consequent pole (CP) PM machines have been extensively studied [4]–[19]. As acclaimed in [4], [5] the flux reversal machine with CP PM stator (CP PM mover) can obtain 26% (21%) higher torque density (thrust density) by saving half amount of PM material. In [6], it was proved that the partitioned stator with CP PM stator can obtained more than 98% torque density by saving 28% PM material. The machine with CP PM rotor can maintain equivalent torque performance and better field-weakening capability [7], [8].

However, the employ of CP PM rotor results in asymmetry air-gap flux density, which lead to even-order back-EMF harmonics, higher torque ripple, serious end magnetization and unbalanced magnetic force (UMF). In [7]–[10], it was pointed out that the even-order back-EMF harmonics caused by the

The associate editor coordinating the review of this article and approving it for publication was Gaolin Wang.

CP PM rotor can be eliminated by employing appropriate combinations of slot and pole. Various technical methods have been employed to reduce detent force and torque (thrust) ripple, including uniform air-gap [8], skewed rotor, eccentric shape CP PMs and modular mover [10]–[12], which results in lower torque density and complicated manufacturing process. Multi-layer winding has been employed to suppression the even-order back-EMF harmonics, resulting complicated winding arrangement and the unipolar leakage flux has not been improved [13].

As reported in [14], the end leakage flux is generated by unbalance magnetic circuit, resulting magnetization of the end shaft and bearing. For the CP PM machine [15], the discrepancy of 2D and 3D FE results are discussed and nonmagnetic material was suggested to suppression the end leakage flux, while the leakage flux has not been suppressed in a real sense. In [16]–[18], a step-staggered CP PM rotor and novel magnetic pole sequence were proposed to reduce the unipolar end leakage flux of the CP PM machine, resulting lower torque density and complicated rotor structure. In [19], the AMP was proposed to suppress the unipolar end leakage flux CP PM machine. While for the CP PM machine which exist even-order back-EMF harmonics in the winding, the EMP and APM can also be employed.

In this paper, the CP EMP and AMP are presented to suppression the even-order back-EMF harmonics as well as the end leakage flux. The 18-slot/20-pole (18/20) machine is employed, which is composed by two 9-slot/10-pole unit machine. The suppression principle of even-order back-EMF harmonics in the EMP and AMP machine is described. The influence of various magnetic pole on the electromagnetic characteristic are discussed. Further, the influence of different CP magnetic pole on the unipolar end leakage flux is investigated.

This paper is organized as follows. Four machine topologies, i.e., traditional SPM, CP PM, CP EMP and CP AMP are described in Section II. In Section III, suppression principle of even back-EMFs harmonics is illustrated by harmonics superposition, as well as the parasitic effect on end leakage flux. In Section IV, the electromagnetic performance together with end leakage flux distribution of the machine with different magnetic pole arrangements are presented. In Section V, the prototype with CP AMP rotor is manufactured and tested to validate the theoretical and FE analysis. Conclusion is given in Section VI.

II. MACHINE TOPOLOGY WITH VARIOUS MAGNETIC POLE STRUCTURE

In order to investigate the influence of various magnetic pole structures on the even back-EMF harmonics, torque ripple reduction as well as end leakage flux, the 18/20 SPM machine is employed for illustration.

The schematic section of traditional and CP SPM machines with concentrated winding are presented as Figs. 1(a) and (b). The structure of CP EMP and AMP SPM machine together with the winding arrangement

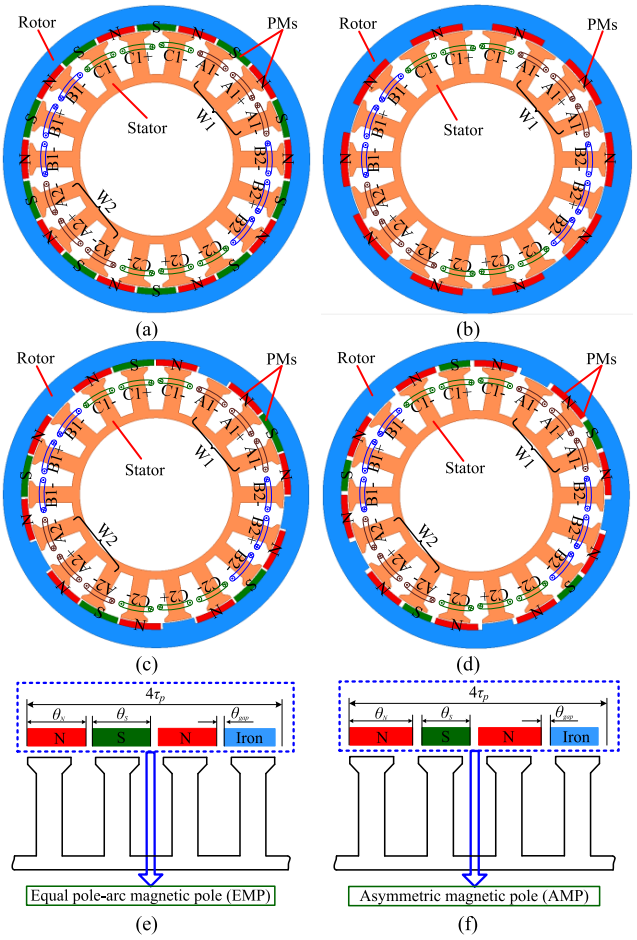

FIGURE 1. Graph of the analyzed machines. (a) 18/20 SPM machine. (b) 18/20 CP SPM machine. (c) 18/20 CP EMP machine (d) 18/20 CP AMP machine. (e), (f) MP structure of EMP and AMP.

are given in Figs. 1(c) and (d), respectively. Whilst the corresponding diagrams of EMP and AMP are given in Figs. 1(e) and (f), respectively. The magnetic pole of the CP EMP and AMP machine are divided into five groups, one group of CP MP is accounted for four times pole pitch, i.e., $4\tau_p$, (τ_p is pole pitch) composed by N-S-N-Iron. As for the CP EMP in Fig. 1(e), the pole-arc angle of N, S magnetic pole and air gap are defined as $q_{N1}\theta_{N1}$, $q_{S1}\theta_{S1}$ and $q_{\text{gap1}}\theta_{\text{gap1}}$, respectively, and the pole-arc angle of N is equal to S magnetic pole. However, for the CP AMP in Fig. 1(f), the pole-arc angle of N, S magnetic pole and air gap are defined as q_{N2}, q_{S2} and q_{gap2}, respectively, and the pole-arc angle of iron core is equal to S magnetic pole. The optimal design structure parameters of the four machines employed in FE analysis are given in Table. 1. The traditional 18/20 SPM, 18/20 CP SPM, 18/20 CP EMP and 18/20 CP AMP machines are indicated with capital symbol I-IV, respectively.

III. EVEN-ORDER BACK-EMF HARMONICS SUPPRESSION PRINCIPLE AND PARASITIC EFFECT ON END LEAKAGE FLUX

The even-order back-EMF harmonics suppression principle for the machine with CP EMP and AMP arrangements will

TABLE 1. Main design parameters of the 18-Slot/20-Pole SPM machine.

Items	I	III	III	IV
Airgap length (mm)		0.5		
Axial length (mm)		30		
Rated speed (r/min)		300		
Rotor outer diameter (mm)		126		
Stator outer diameter (mm)		105		
Stator inner diameter (mm)		63		
Turns in one teeth		30		
Magnet remanence (T)		1.1		
Back-iron (mm)		3.3		
Tooth width (mm)		6.6		
Current density (A/mm^2)		4		
PM thickness (mm)	2.5	2.7	2.5	2.5

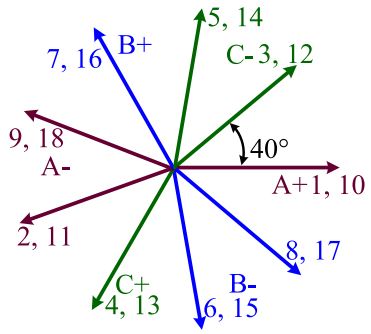

FIGURE 2. Star of slot for the back-EMF phasor of the 18/20 SPM machine.

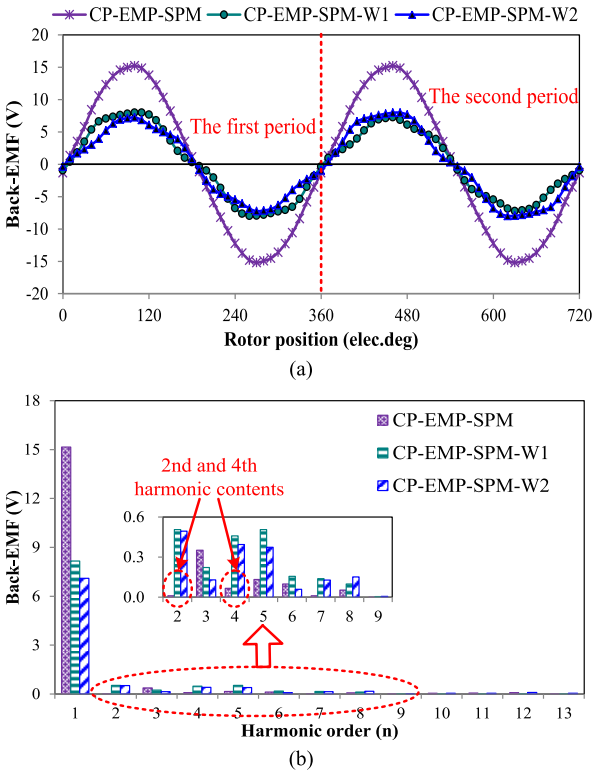

FIGURE 3. Phase back-EMF waveforms and harmonic contents of the CP EMP machine. (a) Waveforms. (b) Harmonic.

be introduced, as well as the parasitic effect of unipolar end leakage flux.

A. EVEN-ORDER BACK-EMF HARMONICS SUPPRESSION PRINCIPLE

For CP PM machine, the even-order back-EMF harmonics exist in the coils due to the unbalance magnetic circuit. Fig. 2 presents the star of slot for the 18/20 SPM machine, it can be observed that the number of back-EMF phasor belongs to one phase is three for one machine periodicity. For the back-EMF phasor belongs to the negative phase band, there does not exist a phasor in the positive phase band which is 180 degrees out of phase, so the even-order back-EMF harmonics cannot be cancelled.

The CP EMP and AMP structures are employed to suppression the even-order back-EMF harmonics, as given in Figs. 1(e) and (f). As described in Figs. 1(a)-(d), the phase winding belongs to the first and the second machine periodicity is defined as W1 and W2, respectively. For the machine with CP EMP rotor, the back-EMF of W1 and W2 winding together with their resultant waveforms are described in Fig. 3(a), whilst the harmonics contents are given in Fig. 3(b). The 2nd and 4th harmonics can be suppressed effectively as depicted in Fig. 3(b).

The suppression principle of 2nd and 4th back-EMF harmonics for the CP EMP machine is explained in Figs. 4(a)-(e), whilst the amplitude and phase in W1 and W2 windings are listed in Table. 2. For the 2nd back-EMF harmonic, the suppression principle can be illustrated as follows.

In the first electric period, compared with the fundamental, the phase of the 2nd back-EMF harmonic in the W1 winding is 4.9 degree, while 185 degree for the 2nd back-EMF harmonic in the W2 winding, the 2nd back-EMF harmonic can be cancelled effectively. In the second electric period, the phase of the 2nd back-EMF harmonic in the W1 and W2 windings reversed each other as the phase in the first electric period. The 2nd back-EMF harmonic waveform of W1 and W2 winding and the resultant waveform are given in Fig. 4(e). The suppression principle of the 4th back-EMF harmonic can be explained as the similar way and the corresponding waveforms are given in Figs. 4(c) and (d), respectively.

B. PARASITIC EFFECT ON END LEAKAGE

Although the PM machine with CP rotor can improve the utilization of PM, one group magnetic poles with the same polarity are removed and replaced by iron core leading to accumulative field, result in unipolar end leakage flux. Fig.5 presents the leakage flux path, which flows through the end shaft and air due to the unbalanced rotor poles. The redundant flux will flow through this path when the iron core is saturate, which result in magnetization of shaft and bearing. The unipolar end leakage flux, which has harmful effect (magnetization of end shaft and bearing) on the safe operation of the machine will discussed in the Section IV-C.

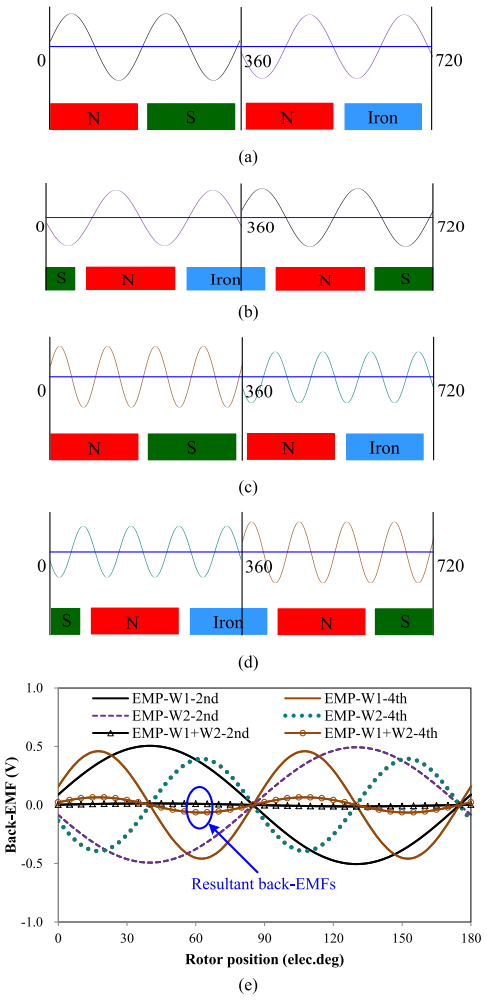

FIGURE 4. Suppression principle of the 2nd and 4th harmonics for the EMP machine. (a), (b) 2nd harmonic in the W1 and W2 windings. (c), (d) 4th harmonic in the W1 and W2 windings. (e) 2nd, 4th and resultant harmonic waveforms in the W1 and W2 windings.

TABLE 2. Amplitude and phase of the harmonics in W1 and W2 windings.

Item (AMP1)	W1		W2		W1+ W2
	Amplitude (V)	Phase (°)	Amplitude (V)	Phase (°)	Amplitude (V)
2nd	0.505	4.85	0.494	185	0.012
4th	0.459	14.90	0.394	195	0.061

IV. ELECTROMAGNETIC PERFORMANCE ANALYSIS

For fair comparison, the width of stator tooth and yoke of CP SPM and CP AMP SPM machine maintain the same as the traditional SPM machine. The pole-arc and thickness of PM are optimized to have a favorable electromagnetic performance. The open circuit flux density distribution and waveforms, torque characteristics, end leakage flux, UMF and efficiency of the four machines will be discussed as follows.

A. OPEN-CIRCUIT FIELD DISTRIBUTION AND BACK-EMFS

Figs. 6(a)-(d) present the open-circuit field distribution of the traditional 18/20 SPM, CP SPM, CP EMP and CP

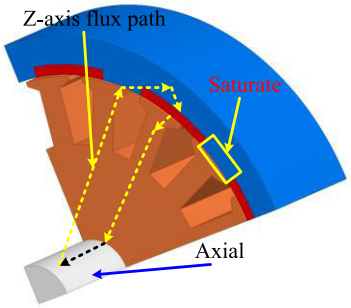

FIGURE 5. Graphics of z-axial unipolar end leakage flux.

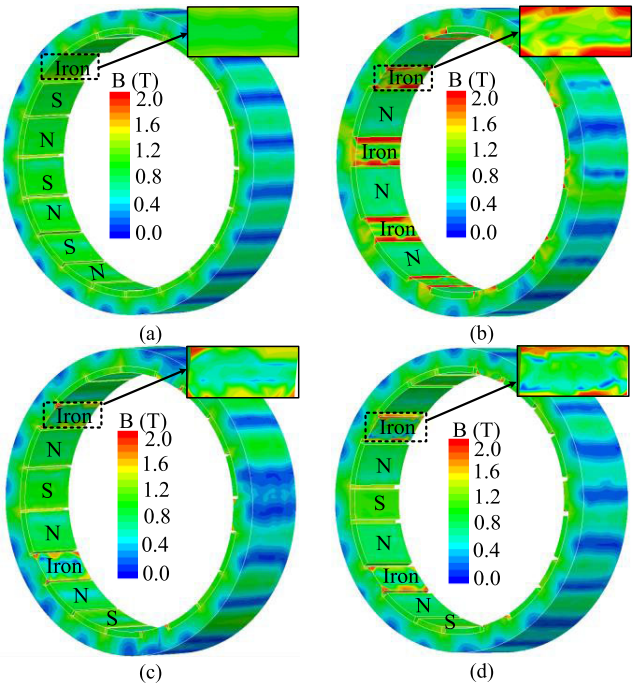

FIGURE 6. Open-circuit flux field distribution of the out rotor for the analyzed machines. (a) 18/20 SPM machine. (b) 18/20 CP SPM machine. (c) 18/20 CP EMP machine. (d) 18/20 CP AMP machine.

AMP machines, respectively. The CP SPM machine demonstrates the maximum flux density in the iron core, while smallest for the traditional SPM machine. The saturate of the iron core will lead to unipolar end leakage flux, which result in magnetization of shaft and bearing, resulting negative influence on the electromagnetic characteristics and security risks of mechanical performance.

Fig. 7(a) presents the open-circuit air-gap flux density waveforms of the analyzed machines, which is the main factor affecting the electromagnetic performance, whilst the harmonic contents are listed in Fig. 7(b). It can be observed that the even-order harmonics exist in the air-gap flux density for the machine with various CP MP rotor owing to the replace of one group of PMs with the same polarity by the iron core. The fundamental is the highest for the traditional SPM machine, while it is smallest for the CP EMP machine; whilst the CP AMP machine can achieve 98.07% of the

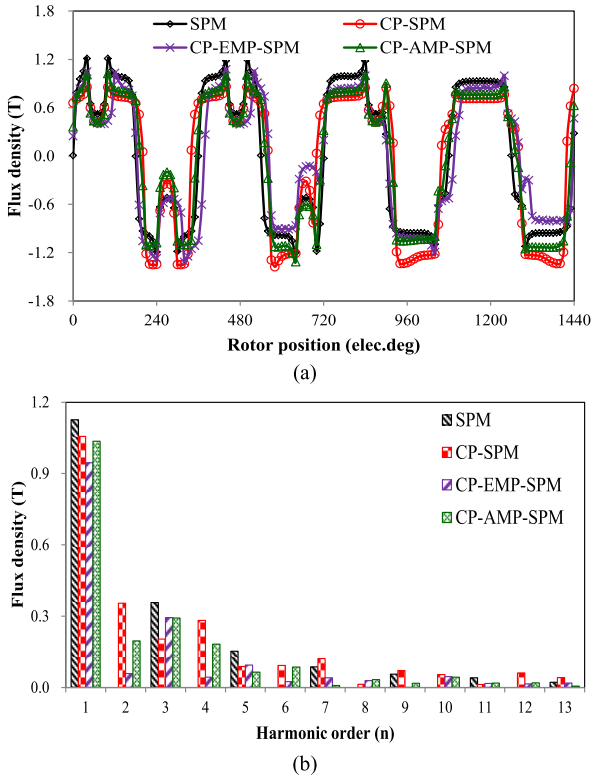

FIGURE 7. Open-circuit airgap flux density. (a) Waveforms. (b) Harmonics.

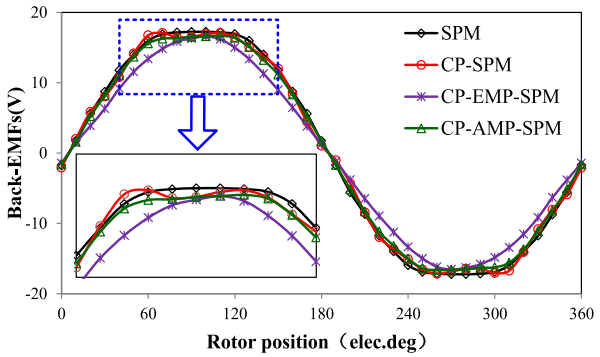

FIGURE 8. FE predicted phase back-EMF waveforms of the analyzed machines (operate at 300r/min).

CP PM machine. Although the amount of PM material is reduced, the fundamental air-gap flux density can keep fairly high for the machine with CP rotor. This phenomenon can be interpreted as the PMs with the same polarity replaced by iron core reduce the reluctance in the magnetic circuit, improving the utilization of PM material.

The back-EMF waveforms and local magnification of the four machines are presented in Fig. 8, and the harmonic contents are listed in Table. 3. As can be observed that the 2nd and 4th back-EMF harmonics can be suppressed by the CP EMP and AMP structure effectively. In addition, the traditional SPM machine has the highest fundamental, while smallest for the machine with CP EMP rotor. It can be seen that the 5th harmonics of the CP AMP machine is the smallest

TABLE 3. Harmonic contents in back-EMF (300r/min).

Harmonic	I	II	III	IV
1	17.59	17.48	15.15	16.86
2	0.00	0.13	0.04	0.05
3	1.39	1.01	0.14	1.18
4	0.00	0.06	0.04	0.04
5	0.17	0.54	0.12	0.22
6	0.00	0.10	0.05	0.15
7	0.12	0.11	0.01	0.10
8	0.00	0.68	0.04	0.05
9	0.00	0.00	0.01	0.00
10	0.00	0.09	0.02	0.05
11	0.01	0.04	0.05	0.01
12	0.00	0.06	0.11	0.04
13	0.02	0.03	0.01	0.01

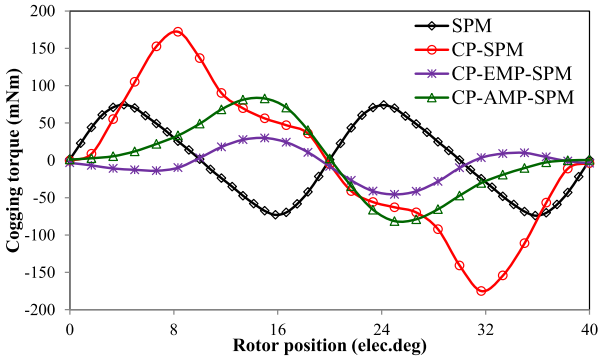

FIGURE 9. FE predicted cogging torque waveforms.

of the machines, and the 7th harmonic can be reduced by 90.9% compared with the machine with CP PM rotor. The 5th harmonics of the CP AMP machine can be reduced by 59.3%, while remains almost the same for the 7th harmonic compared with the CP SPM machine.

B. TORQUE CHARACTERISTICS

The cogging torque has negative influence on the vibration and noise of the PM machine, the cogging torque waveforms are given in Fig. 9. As pointed out in [13], for the machines with N_S slots and P pole pairs, the number of cogging torque period is the least common multiple of the number of slot (N_S) and pole ($2P$). While it is the least common multiple of the number of slot (N_S) and pole pairs (P) for the machine with CP PM rotor. For the 18/20 PM machine with CP rotor, the cogging torque period is double times of the traditional SPM machine. This can be verified by the cogging torque waveforms in Fig. 9. As can be seen that the machine with CP EMP rotor has the minimum cogging torque, while maximum for the machine with CP PM rotor. The peak cogging torque of the four machines is listed in Table. 4, in which T_{cog} is the peak of cogging torque.

The electromagnetic torque waveforms of the four machines are given in Fig. 10, whilst the torque characteristics, volume of PM and torque density of PM material are listed in Table. 4. T_{ripple}, T_{avg} and V_{PM} are the torque ripple, average electromagnetic torque and volume of PM for the

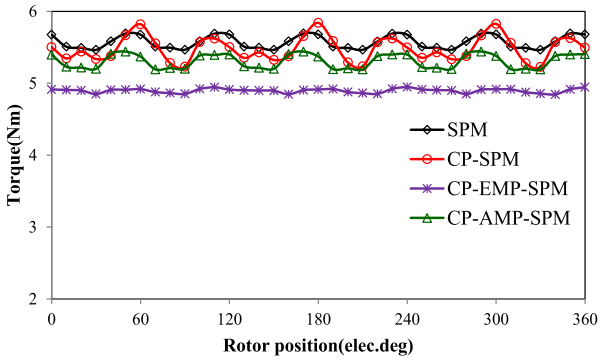

FIGURE 10. Variation of electromagnetic torque with rotor position (BLAC, $i_d = 0$, slot current RMS density $J = 4\text{A/mm}^2$).

TABLE 4. Torque characteristics and volume of PM for the analyzed machines.

Items	I	II	III	IV
6th (Nm)	0.09	0.17	0.03	0.10
12th (Nm)	0.02	0.02	0.01	0.01
T_{cog} (mNm)	52.1	176.8	43.0	47.5
T_{ripple} (%)	3.68	10.31	2.29	4.84
T_{avg} (Nm)	5.24	5.18	4.55	5.01
V_{PM} (cm^3)	23.86	17.82	19.17	18.14
η_{PM} (Nm/cm^3)	0.2196	0.2906	0.2373	0.2762

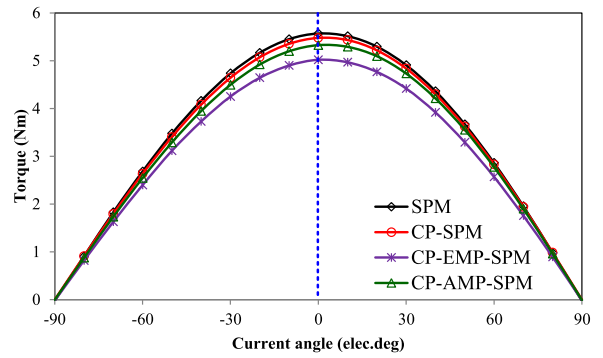

FIGURE 11. Average electromagnetic torque versus current angle for the four machines.

four machines. Compared with the traditional SPM machine, the machine with CP PM, CP EMP and CP AMP rotor can achieve 98.85%, 86.83% and 95.61% torque density by saving 25.31%, 19.66% and 23.97% amount of PM material, respectively. As for the torque ripple, it can be seen that the machine with CP EMP rotor has the smallest torque ripple while highest for the machine with CP PM rotor, the torque ripple of the machine with CP AMP rotor is 5.47% lower than the CP SPM machine.

The average electromagnetic torque versus current angle of the four machines is given in Fig. 11. As can be seen that the four machines can achieve the maximum average torque when the machines are operated under the zero d-axis current control, i.e., $i_d = 0$. The reluctance torque is negligible for the machine with CP PM rotor.

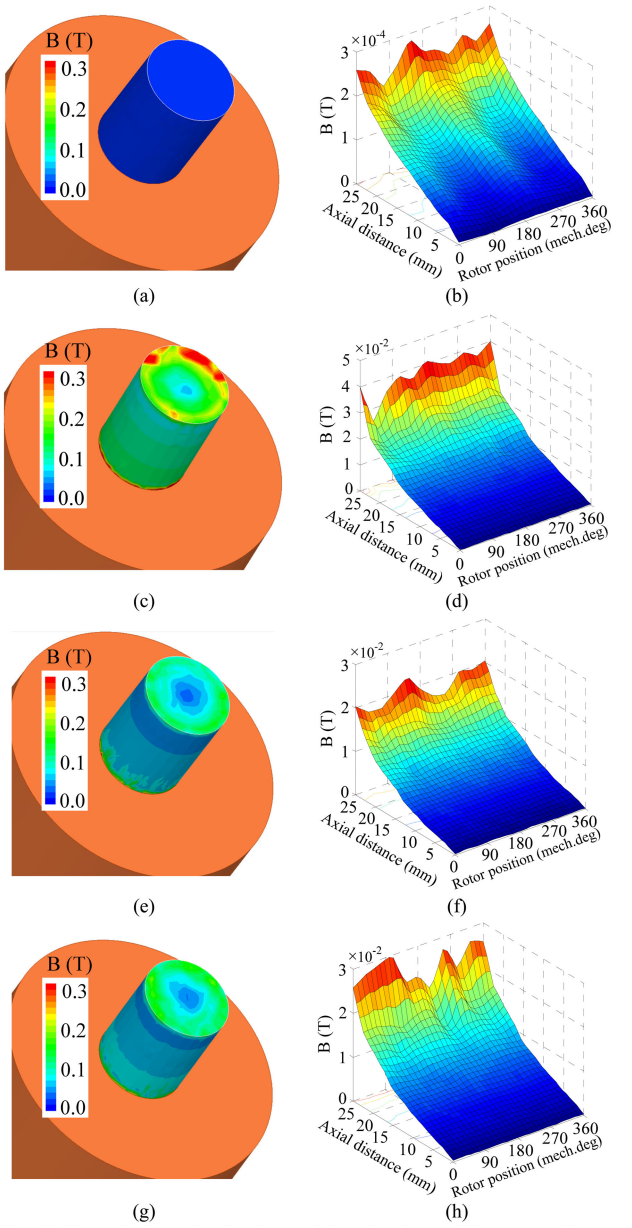

FIGURE 12. Magnetic field distribution and flux density at different position of end shaft for the four machines. (a), (b) 18/20 SPM machine. (c), (d) 18/20 CP SPM machine. (e), (f) 18/20 CP EMP machine. (g), (h) 18/20 CP AMP machine.

C. REDUCTION OF UNIPOLAR END LEAKAGE FLUX

The unipolar leakage flux may causes magnetization of the end shaft and bearing, resulting unreliable operation of the machine. In order to illustrate the end leakage flux distribution of the four machines, the end shaft is limited in 25mm. The flux density distribution on the surface of end shaft of the four machines is shown in Figs. 12(a), (c), (e) and (g), respectively, and the corresponding flux density at different positions is given in Figs. 12(b), (d), (f) and (h), respectively. It can be observed that the unipolar end leakage flux distribution is serious (around 0.0121T in average) in the CP SPM

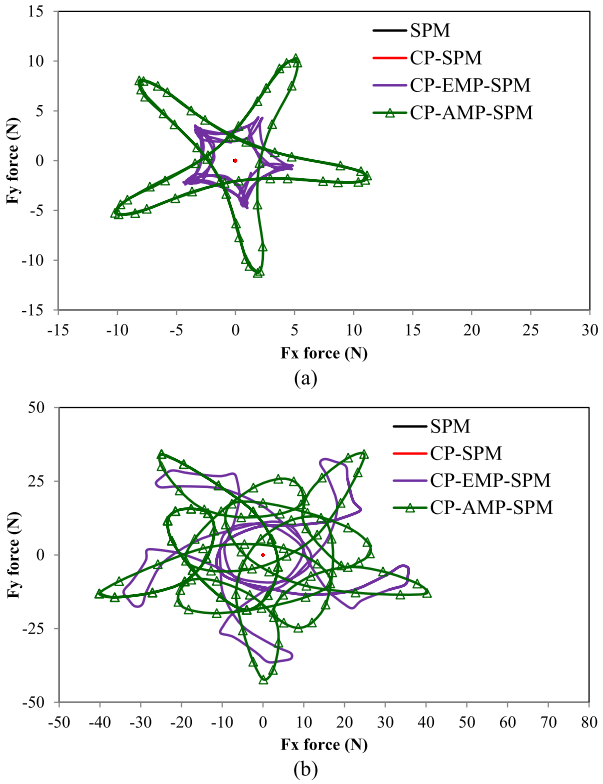

FIGURE 13. UMF in open-circuit and rated load. (a) Open-circuit. (b) Rated load.

machine compared with the traditional SPM machine. However, the unipolar leakage flux can be reduced by 0.0054T and 0.0034 (in average) for the machine with EMP and AMP CP PM rotor. It can be observed that the flux density increases with the axial distance, and the maximum leakage flux density exist in the end shaft of the machine. The maximum leakage flux density is up to 0.0412T for the machine with CP rotor, while 0.0230 T and 0.0300T for the CP EMP and AMP machine, respectively. The unipolar leakage flux of CP PM machine can be suppressed by the AMP structure, further reduce the magnetization of the end shaft.

D. UMF

The machine with CP PM rotor, which features with high utilization of PM material, suffering the unbalanced magnetic force (UMF) for the special combination of slot and pole [6], [10]. The UMF under open-circuit and rated load of the four machines are shown in Figs. 13(a) and (b), respectively. There does not exists UMF for the traditional SPM and CP PM machines, while the UMF exist for the machine with CP EMP and AMP rotor whether the machines operate in open-circuit or rated load. The loci of the UMF for the machine with CP EMP and AMP rotor is different, in addition, the amplitude of UMF on rated load is higher than that in open-circuit. The UMF of machine with CP EMP and AMP can be explained as: although the 18/20 machine composed by two unit machine, while the magnetic pole arrangement of AMP change the symmetry of the machine. It should be noted that the UMF in the machine with CP AMP rotor will be cancelled out by multiplying both the slot and pole.

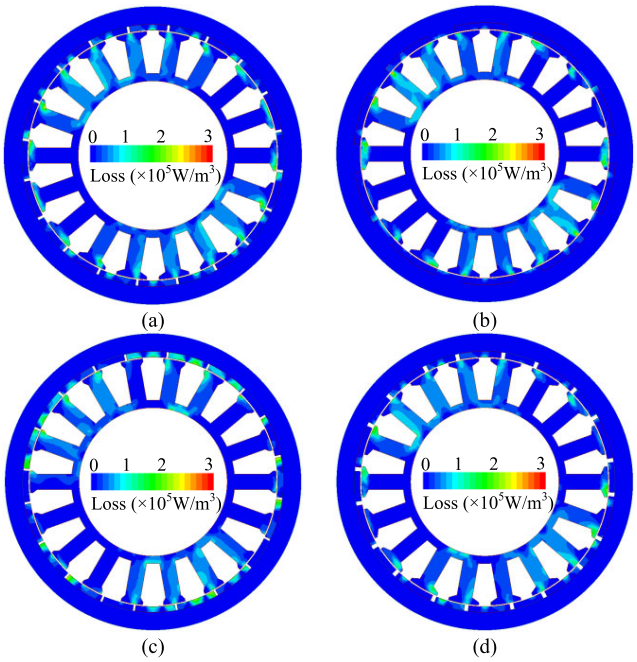

FIGURE 14. Loss maps of the machines. (a) 18/20 SPM machine. (b) 18/20 CP SPM machine. (c) 18/20 CP EMP machine. (d) 18/20 CP AMP machine.

TABLE 5. Iron loss, PM eddy current loss and efficiency of the machines.

Items	I	II	III	IV
Iron loss (W)	2.78	3.08	2.26	2.72
PM loss (W)	0.46	0.20	0.98	0.32
Copper (W)	18.87			
Power (W)	164.60	162.72	142.93	157.38
η (%)	88.1	88.0	86.6	87.8

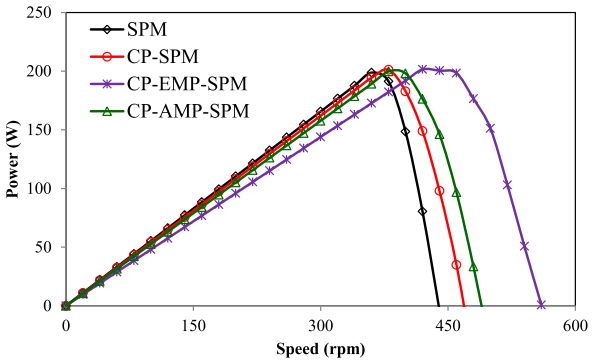

FIGURE 15. FE calculated power-speed curve.

E. LOSS, POWER-SPEED ENVELOP AND EFFICIENCY

The iron loss and PM eddy current loss of the four machines are predicted under rated phase current (peak 6.3A) at 300r/min. The loss maps of the machine are shown in Figs. 14(a)-(d), respectively, whilst the iron loss, PM eddy current loss, copper loss and efficiency are listed in Table. 5, η is the efficiency of the machine. It can be observed that

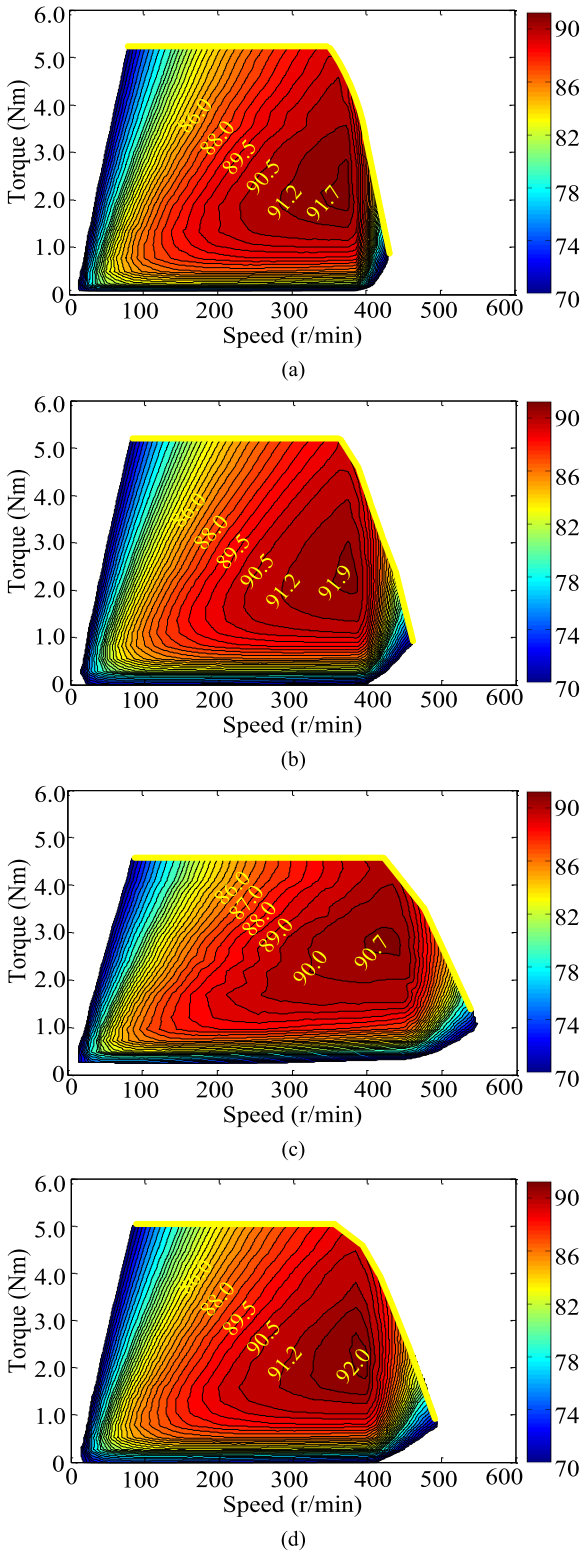

FIGURE 16. Efficiency maps of the four machines. (a) 18/20 SPM machine. (b) 18/20 CP SPM machine. (c) 18/20 CP EMP machine. (d) 18/20 CP AMP machine.

the SPM machine has the largest efficiency, while it is the smallest for the CP EMP machine.

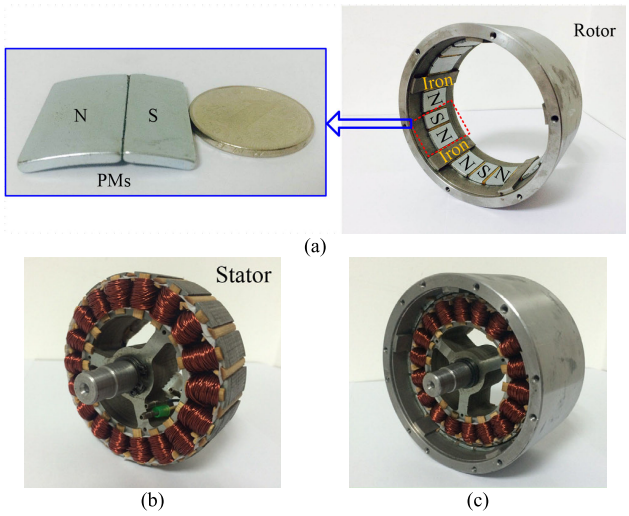

FIGURE 17. CP AMP prototype machine. (a) APM PMs and CP AMP rotor. (b) Stator. (c) Assembled stator and CP AMP rotor.

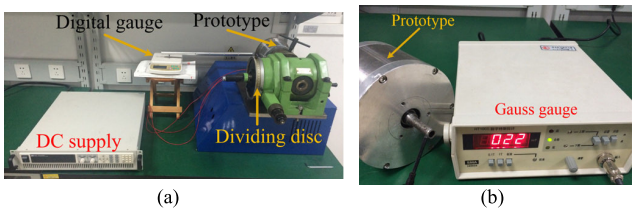

FIGURE 18. Static torque and end leakage flux test platform. (a) Static torque test rig. (b) End leakage flux test rig.

The power-speed curves and efficiency of the four machines are further discussed as follows. With the identical limitation on dc bus voltage (42V) and rated phase current, the power-speed curve of the four machines are predicted and shown in Fig. 15. It can be noted that the four machines can achieve the similar maximum power when operated in different speed. The maximum operate speed of the CP EMP machine is the largest, while smallest for the traditional SPM machine.

Fig. 16 shows the efficiency contour maps of the four machines, they are predicted under the same limitation conditions as the power-speed curve. It can be observed that CP EMP machine can achieve the best flux-weakening ability, this is due to its back-EMF at 300r/min is smallest (as shown in Fig. 8) of the machines whilst the efficiency contour maps are calculated under the same dc bus voltage. It can also be noted that the AMP PM machine can achieve the maximum efficiency, which is 0.3% higher than the SPM machine. Although the flux-weakening ability of the EMP machine is the best, while its efficiency is the smallest.

V. EXPERIMENTAL VERIFICATION

The 18/20 machine with CP AMP rotor is manufactured to confirm the suppression effect of even-order back-EMF harmonics and unipolar end leakage flux. The 20-pole CP

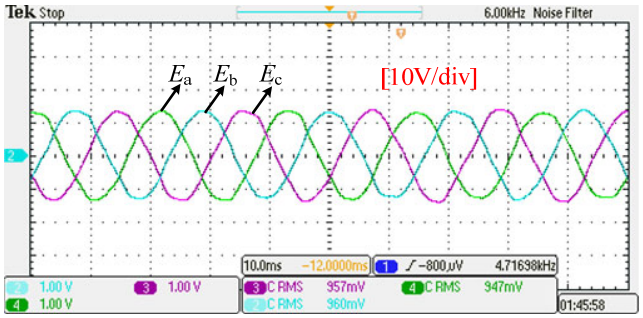

FIGURE 19. Measured back-EMF waveforms (operate at 300r/min).

TABLE 6. Measured and FE predicted harmonic contents in back-EMF.

	18/20 CP AMP2 SPM machine				
Items	2-D	MEA	Items	2-D	MEA
1	100 (16.86)	100 (15.02)	8	0.29	0.24
2	0.27	0.25	9	0.00	0.00
3	7.02	6.59	10	0.32	0.28
4	0.24	0.22	11	0.06	0.05
5	1.33	1.21	12	0.22	0.24
6	0.91	0.71	13	0.09	0.11
7	0.62	0.52			

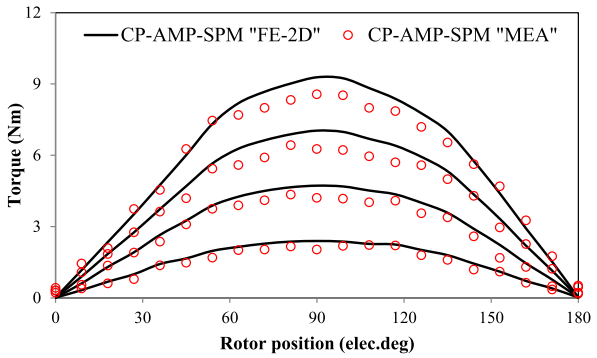

FIGURE 20. Comparison of measured and FE predicted static torque ($I_{dc} = I_a/2 = -I_b = -I_c$).

AMP rotor and the PMs is shown in Fig. 17(a), whilst the stator and assembled machine are given in Figs. 17(b) and (c). The static torque test platform is presented in Fig. 18(a), and end leakage flux is tested by the gauss gauge, as presented in Fig. 18(b).

Fig. 19 presents the measured phase back-EMF waveforms by driving the out rotor at 300r/min. Meanwhile the waveforms are analyzed with Fourier transform; the results of the FE predicted and measured are compared in Table. 6. The measured 2nd and 4th harmonics has a good agreement with the FE predicted, this indicate that the AMP structure can be an effectiveness technique to cancel the even-order back-EMF harmonics.

The static torque of the prototype is measured by suppling the dc current with $I_{dc} = I_a/2 = -I_b = -I_c$, as presented in Fig. 20. The measured static torque is lower than that of the FE predicted due to the machining error and end effect.

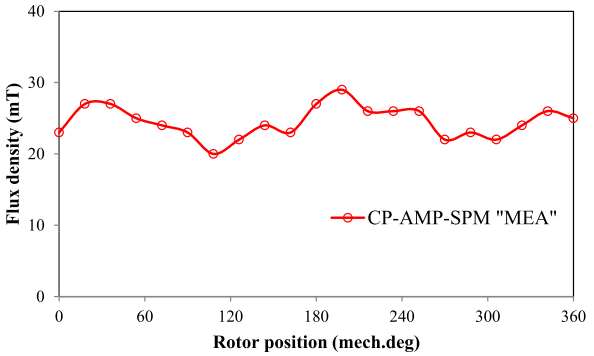

FIGURE 21. Tested end leakage flux of the prototype machine.

Fig. 21 presents the measured leakage flux, which is tested on the end shaft, it can coincide well with the FE predicted in Fig. 12(h).

VI. CONCLUSION

The CP EMP and AMP arrangements are proposed to suppression the even-order harmonics and end leakage flux. The cancellation principle of even-order back-EMF harmonics was introduced by harmonic superposition principle. The electromagnetic performance of machines with various magnetic pole structure, including back-EMF, torque characteristics, unipolar end leakage flux, UMF, loss and efficiency are investigated in detail. It is found that the even-order back-EMFs harmonics can be suppressed effectively for the machines with CP EMP and AMP structure. The torque ripple of machines with CP EMP and AMP is 8.02% and 5.47% lower than CP PM machine, whilst maintain 86.83% and 95.61% torque density. In addition, the unipolar end leakage flux can be suppressed by employing CP EMP and AMP structure. Further, the flux-weakening ability of the CP EMP is the best, while its maximum efficiency is the lowest of the machines. The prototype machine with CP AMP rotor is fabricated and measured to confirm the theoretical analyses and FE results.

REFERENCES

[1] A. M. El-Refaie, "Fractional-slot concentrated-windings synchronous permanent magnet machines: Opportunities and challenges," *IEEE Trans. Ind. Electron.*, vol. 57, no. 1, pp. 107–121, Jan. 2010.

[2] X. Sun, B. Su, S. Wang, Z. Yang, G. Lei, J. Zhu, Y. Guo, "Performance analysis of suspension force and torque in an IBPMSM with V-shaped PMs for flywheel batteries," *IEEE Trans. Magn.*, vol. 54, no. 11, Nov. 2018, Art. no. 8105504.

[3] I. Boldea, L. N. Tutelea, L. Parsa, and D. Dorrell, "Automotive electric propulsion systems with reduced or no permanent magnets: An overview," *IEEE Trans. Ind. Electron.*, vol. 61, no. 10, pp. 5696–5711, Oct. 2014.

[4] Y. Gao, R. Qu, D. Li, J. Li, and G. Zhou, "Consequent-pole flux-reversal permanent-magnet machine for electric vehicle propulsion," *IEEE Trans. Appl. Supercond.*, vol. 26, no. 4, Jun. 2016, Art. no. 5200105.

[5] S.-U. Chung, H.-J. Lee, and S.-M. Hwang, "A novel design of linear synchronous motor using FRM topology," *IEEE Trans. Magn.*, vol. 44, no. 6, pp. 1514–1517, Jun. 2008.

[6] Z. Z. Wu and Z. Q. Zhu, "Partitioned stator flux reversal machine with consequent-pole PM stator," *IEEE Trans. Energy Convers.*, vol. 30, no. 4, pp. 1472–1482, Dec. 2015.

[7] S.-U. Chung, J.-W. Kim, Y.-D. Chun, B.-C. Woo, and D.-K. Hong, "Fractional slot concentrated winding PMSM with consequent pole rotor for a low-speed direct drive: Reduction of rare earth permanent magnet," *IEEE Trans. Energy Convers.*, vol. 30, no. 1, pp. 103–109, Mar. 2015.
[8] S.-U. Chung, S.-H. Moon, D.-J. Kim, and J.-M. Kim, "Development of a 20-pole–24-slot SPMSM with consequent pole rotor for in-wheel direct drive," *IEEE Trans. Ind. Electron.*, vol. 63, no. 1, pp. 302–309, Jan. 2016.
[9] J. Asama, M. Amada, M. Takemoto, A. Chiba, T. Fukao, and A. Rahman, "Voltage characteristics of a consequent-pole bearingless PM motor with concentrated windings," *IEEE Trans. Magn.*, vol. 45, no. 6, pp. 2823–2826, Jun. 2009.
[10] S.-U. Chung, J.-M. Kim, D.-H. Koo, B.-C. Woo, D.-K. Hong, and J.-Y. Lee, "Fractional slot concentrated winding permanent magnet synchronous machine with consequent pole rotor for low speed direct drive," *IEEE Trans. Magn.*, vol. 48, no. 11, pp. 2965–2968, Nov. 2012.
[11] F. Li, K. Wang, J. Li, H. Y. Sun, and P. C.-K. Luk, "Electromagnetic performance analysis of PMSM with eccentric consequent pole rotor," in *Proc. IEEE PESA*, Hongkong, Dec. 2017, pp. 1–7.
[12] S.-U. Chung, J.-W. Kim, B.-C. Woo, D.-K. Hong, J.-Y. Lee, and D.-H. Koo, "Force ripple and magnetic unbalance reduction design for doubly salient permanent magnet linear synchronous motor," *IEEE Trans. Magn.*, vol. 47, no. 10, pp. 4207–4210, Oct. 2011.
[13] F. Li, K. Wang, J. Li, and H. J. Zhang, "Suppression of even-order harmonics and torque ripple in outer rotor consequent-pole PM machine by multilayer winding," *IEEE Trans. Magn.*, vol. 54, no. 11, Nov. 2018, Art. no. 8108605.
[14] Z. Q. Zhu, H. Hua, A. Pride, R. Deodhar, and T. Sasaki, "Analysis and reduction of unipolar leakage flux in series hybrid permanent-magnet variable flux memory machines," *IEEE Trans. Magn.*, vol. 53, no. 11, Nov. 2017, Art. no. 2500604.
[15] S.-U. Chung, J.-W. Kim, B.-C. Woo, D.-K. Hong, J.-Y. Lee, and D.-H. Koo, "A novel design of modular three-phase permanent magnet Vernier machine with consequent pole rotor," *IEEE Trans. Magn.*, vol. 47, no. 10, pp. 4215–4218, Oct. 2011.
[16] X. Ge, Z. Q. Zhu, J. Li, and J. Chen, "A spoke-type IPM machine with novel alternate airspace barriers and reduction of unipolar leakage flux by step-staggered rotor," *IEEE Trans. Ind. Appl.*, vol. 52, no. 6, pp. 4789–4797, Nov./Dec. 2016.
[17] K. Wang, J. Li, S. S. Zhu, and C. Liu, "Novel hybrid-pole rotors for consequent-pole PM machines without unipolar leakage flux," *IEEE Trans. Ind. Electron.*, vol. 66, no. 9, pp. 6811–6823, Sep. 2019.
[18] J. Li, K. Wang, F. Li, S. S. Zhu, and C. Liu, "Elimination of even-order harmonics and unipolar leakage flux in consequent-pole PM machines by employing N-S-Iron–S-N-iron rotor," *IEEE Trans. Ind. Electron.*, vol. 66, no. 3, pp. 1736–1747, Mar. 2019.
[19] F. Li, K. Wang, J. Li, and H. Y. Sun, "Electromagnetic performance analysis of consequent-pole PM machine with asymmetric magnetic pole," *IEEE Trans. Magn.*, vol. 55, no. 6, Jun. 2019, Art. no. 8103205.

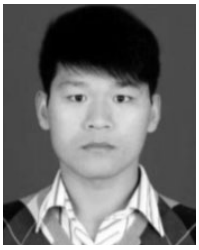

FENG LI received the B.S. degree in electrical engineering from the Wanfang College of Science and Technology, Jiaozuo, China, in 2012, and the M.S. degree in electrical engineering from Henan Polytechnic University, Jiaozuo, in 2015. He is currently pursuing the Ph.D. degree in electrical engineering with Nanjing University of Aeronautics and Astronautics, Nanjing, China. His current research interests include the design and analysis of permanent magnet machines.

KAI WANG (M'13–SM'14) received the B.Eng. degree from China Jiliang University, Hangzhou, China, in 2004, and the Ph.D. degree from Zhejiang University, Hangzhou, in 2009. From 2009 to 2010, he was with the Memorial University of Newfoundland, St. John's, NL, Canada, as a Postdoctoral Fellow. From 2010 to 2013, he was with The University of Sheffield, Sheffield, U.K. From 2013 to 2015, he was a Research Associate with the Sheffield Siemens Wind Power Research Centre, Sheffield, and a Research and Development Engineer with Ansys Inc., Canonsburg, PA, USA. Since 2015, he has been with the College of Automation Engineering, Nanjing University of Aeronautics and Astronautics, Nanjing, China. His current research interests include the design and control of permanent-magnet machines.

HAIYANG SUN received the B.Eng. degree from the Huaihai Institute of Technology, Jiangsu, China, in 2015. He is currently pursuing the Ph.D. degree with the Department of Electrical Engineering, Nanjing University of Aeronautics and Astronautics, Nanjing, China. His research interests include the design and analysis of permanent-magnet machines.

JINWANG KONG received the B.Eng. degree from Yangzhou University, Yangzhou, China, in 2018. He is currently pursuing the master's degree with the Department of Electrical Engineering, Nanjing University of Aeronautics and Astronautics, Nanjing, China. His current research interests include the fault-tolerant control of the five-phase PMSM.